

Precision microwave dielectric and magnetic susceptibility measurements of correlated electronic materials using superconducting cavities

Z. Zhai, C. Kusko, N. Hakim and S. Sridhar

Physics Department, Northeastern University, 360 Huntington Avenue,
Boston, MA 02115

October 23, 2018

Abstract

We analyze microwave cavity perturbation methods, and show that the technique is an excellent, precision method to study the dynamic magnetic and dielectric response in the GHz frequency range. Using superconducting cavities, we obtain exceptionally high precision and sensitivity for measurements of relative changes. A dynamic electromagnetic susceptibility $\tilde{\zeta}(T) = \zeta' + i\zeta''$ is introduced, which is obtained from the measured parameters: the shift of cavity resonant frequency δf and quality factor Q . We focus on the case of a spherical sample placed at the center of a cylindrical cavity resonant in the TE_{011} mode. Depending on the sample characteristics, the magnetic permeability $\tilde{\mu}$, the dielectric permittivity $\tilde{\epsilon}$ and the complex conductivity $\tilde{\sigma}$ can be extracted from $\tilde{\zeta}_H$.

A full spherical wave analysis of the cavity perturbation indicates that : (i) In highly insulating samples with dielectric constant $\epsilon' \sim 1$, the measured $\tilde{\zeta}_H \approx \tilde{\chi}_M$, enabling direct measurement of the magnetic susceptibility. The sensitivity of the method equals or surpasses that of dc SQUID measurements for the relative changes in magnetic susceptibility. (ii) For moderate $\tilde{\epsilon}$ and conductivity σ , $\tilde{\zeta}_H \propto \tilde{\epsilon} + i\omega\tilde{\sigma}/\epsilon_0 - 1$, thus enabling direct measurement of the sample dielectric constant $\tilde{\epsilon}$, even though the sample is placed in a microwave magnetic field. (iii) For large σ we recover the surface impedance limit. (iv) Expressions are provided for the general case of a lossy dielectric represented by $\tilde{\epsilon} + i\omega\tilde{\sigma}/\epsilon_0$. We show that an inversion procedure can be used to obtain $\tilde{\epsilon} + i\omega\tilde{\sigma}/\epsilon_0$ in a wide range of parameter values.

This analysis has led to the observation of new phenomena in novel low dimensional materials. We discuss results on magneto-dynamics of the 3-D antiferromagnetic state of spin chain compound Sr_2CuO_3 . In dielectric susceptibility measurements in $Sr_{14}Cu_{24}O_{41}$, we directly observe a dielectric loss peak. Dimensional resonances in the paraelectric material $SrTiO_3$ are shown to occur due to the rapid increase of dielectric constant with decreasing temperature. The cavity perturbation methods are thus an extremely sensitive probe of charge and spin dynamics in electronic materials.

I Introduction

The continuing discovery of new electronic materials calls for new methods of measuring their electric and magnetic properties. Microwave cavity perturbation techniques have proved to be very useful for the study of transport dynamics at microwave frequencies[1, 2, 3, 4], in materials such as semiconductors, magnetic ferrites and exotic materials such as Charge and Spin Density Waves [5].

In all of these previous studies normal metal cavities were used. To study the (then) newly discovered high temperature superconductors (HTS), the use of superconducting cavities was introduced by Sridhar and Kennedy[1]. The reduction in background absorption by a factor of 10^4 from a normal metal cavity enabled the measurement of absorption in small, single crystal superconductors and thin films. The surface impedance $\tilde{Z}_s = R_s - iX_s$ was obtained in terms of changes of the cavity parameters : the shift in frequency δf and quality factor Q . Subsequently the concept of the “hot

finger” technique introduced in [1] has been used in measurements in other laboratories also with the purpose of studying HTS [6, 7].

In this paper, we present a reanalysis of the cavity perturbation technique, and describe a new application utilizing superconducting microwave cavities, to study dynamic electric and magnetic susceptibilities of strongly correlated electronic materials. We focus on the configuration where the sample is placed at a microwave magnetic field maximum of the TE_{011} mode.

1. We introduce an electromagnetic susceptibility $\tilde{\zeta} = \zeta' + i\zeta''$, which provides a useful framework to discuss the results of the microwave measurements. We use $\tilde{\zeta}_H$ to note the case where the sample is measured in a microwave magnetic field (e.g. in the TE_{011} mode), and $\tilde{\zeta}_E$ when the sample is placed in a microwave electric field (e.g. in the TM_{010} mode). Depending on sample properties, the measured parameter $\tilde{\zeta}$ can be related to the sample magnetic permeability ($\tilde{\mu} = 1 + \tilde{\chi}_M$) and dielectric permittivity ($\tilde{\varepsilon} = 1 + \tilde{\chi}_P$), where $\tilde{\chi}_M$ ($\tilde{\chi}_E$) are the magnetic(electric) susceptibilities, the conductivity $\tilde{\sigma}$ and the surface impedance Z_s . These various limits are discussed in detail in the paper.
2. For highly insulating samples with $\tilde{\varepsilon} \sim 1$, the technique is a very sensitive method of measuring the magnetic susceptibility, since $\tilde{\zeta} \sim \tilde{\chi}_M = \chi'_M + i\chi''_M$. The sensitivity of this technique is compared with others, and it is shown that the microwave method, when superconducting cavities are used, can equal or even exceed that of a dc SQUID for relative changes in susceptibility, such as with changing T . It also yields results on samples (typically mm-sized) in which comparable ac susceptibility measurements do not have sufficient sensitivity. As an example of this technique we show that it yields information on magnetodynamics in a spin chain material Sr_2CuO_3 .
3. When the sample conductivity or dielectric constant is substantial, the measurements are dominated by these parameters. For insulating samples with even moderate dielectric constants ε' , the experiments are a direct measurement of $\tilde{\varepsilon} = \varepsilon' + i\varepsilon''$. *Thus we are able to measure $\tilde{\varepsilon}$ even though the sample is placed in a microwave magnetic field maximum.* (In fact the H_ω field measurements of $\tilde{\varepsilon}$ have an advantage over E_ω measurements as they are not subject to the so-called depolarization peak). We describe an inversion procedure to obtain the complex dielectric constant $\tilde{\varepsilon} + i\tilde{\sigma}/\omega\varepsilon_0$ from the measured data. A spectacular example of the dielectric measurements is the observation of a dielectric loss peak in $\varepsilon''(T)$ due to dielectric relaxation in the spin ladder compound $Sr_{14}Cu_{24}O_{41}$.
4. For sufficiently large ε' , dimensional resonances can occur when the microwave essentially enter into the sample. An striking example of this is presented in data on $SrTiO_3$.
5. When the conductivity σ is appreciable, it can lead to an eddy current contribution resulting in a peak in absorption with increasing conductivity. (This is the magnetic analog of the so-called depolarization peak for E_ω field measurements). For large conductivity the results tend to the surface impedance limit. This is the limit used in previous measurements of the surface impedance of metals and superconductors. This paper presents a unified approach which encompasses both the insulating and highly metallic limits.

The cavity perturbation method discussed here yields unique information on spin and charge dynamics at short time scales between Neutron Scattering and NMR and μSR , and has led to the observation of some unique phenomena in quantum magnets, dielectrics and superconductors.

II Description of apparatus and measurement technique

A right cylindrical cavity (inner radius $7/8$ inch and axial length 1 inch) was made of pure Niobium (Nb), which is a superconductor below $T_c = 9.2K$. The cavity was fabricated in three pieces: two end plates with the needed holes and one center ring. The top plate has a center pumping hole (3.56 mm diameter), and two coupling holes (3.56 mm diameter), the bottom plate has one centrally located hole (6.7 mm diameter), through which the sample is inserted into the cavity. The TE_{011}

mode is degenerate with the TM_{111} mode. As TE_{011} is the desired operating mode, the diameter of these coupling holes was chosen to provide enough perturbation to split the two modes more than $40MHz$ apart. The high quality Nb stock was carefully machined at very low speed to the needed shape and then polished without lubricant, which would otherwise cause oxidation on the Nb surface. Each piece was then annealed, and the grains, which grew due to annealing, vary from sub millimeter size to roughly $4mm$ diameter. The three-piece cavity was tightly held by a stainless steel assembly consisting of a top ring, a center piece for alignment and a bottom ring. The whole resonator was then mounted in an alignment frame, supported on the top by a stainless steel dewar probe ($10.16cm$ diameter and $1m$ long) and, on the bottom, with a sealed copper cup ($10.16cm$ diameter and $10.16cm$ long) with a removable bottom copper plate. Indium seals were used so that the entire assembly were vacuum tight. Superconducting operation of the cavity was accomplished using a bath of liquid 4He .

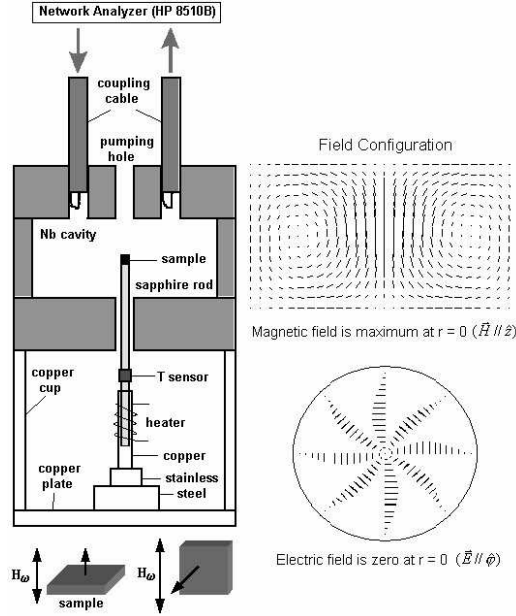


Figure 1: (Left) Diagram for 10GHz superconducting cavity resonant, showing the sample location and the hot finger arrangement to vary sample temperature, while keeping the cavity walls at the bath temperature. By varying sample orientation with respect to H_ω as shown, the anisotropic response can also be measured. (Right) Field configuration in the TE_{011} mode. Also shown is the (top) H_ω field lines in the (r, z) plane plane, and (bottom) E_ω fields at the central $(r, \theta, z = L/2)$ plane of the cavity. For this mode the sample is located at the H_ω field maximum, and at $E_\omega = 0$.

A small piece of sample was mounted on the top of a sapphire rod ($1.56mm$ diameter \times $52mm$ long) using very little Apiezon-N grease. The anisotropic response of the sample can be measured by mounting the sample in different orientations with respect to the applied microwave field for a given mode, as shown in the set-up diagram (Fig. 1). The sapphire rod with sample was inserted into the cavity, along its axis from the bottom, such that the sample is stationed exactly at the center of the cavity. Support and adjustment of the sapphire rod was provided by a copper tube ($20mm$ long), the overlap between copper tube and sapphire rod is adjustable and finally fixed with GE-Varnish to guarantee good thermal contact. The copper tube was brazed at the end to a $6.35mm$ diameter stainless tube (wall thickness $0.15mm$), and the stainless tube was brazed to the bottom copper plate to form a thermal path to the bottom plate which is in contact with liquid 4He .

To heat the sample to higher temperature, a 50Ω heating coil ($0.1mm$ Nichrome wire of

6.5 $\Omega/ft.$) was wound around the copper tube, and the control of the sample temperature was accomplished using an external temperature controller (Lake Shore DRC 82C), with a Silicon Diode temperature sensor (Lake Shore DT 470) which is attached to the sapphire rod outside the cavity. Another temperature sensor is put in the Helium chamber to monitor the bath temperature.

Microwaves were generated with a HP8510B network analyzer, a HP8341B synthesized sweeper and a HP8516A reflection/transmission test set, and coupled into and out of the resonator from the top, through two adjustable 50Ω coaxial lines, each terminated in a loop. One very useful feature of the design is the ability to vary the coupling to the resonator by moving the lines in and out along the axis of the resonator. Thus it is possible to achieve critical coupling and weak coupling over a wide range of the resonator quality factor Q ($10^4 - 10^8$). For fixed coupling, input microwave power can be easily varied and the nonlinear effect of the some samples can be observed[8, 9]. The resonant cavity operated at desired TE_{011} mode has the highest quality factor Q about 2×10^8 at $2K$ bath temperature.

III Electrodynamic basis of the measurement

A small sample of volume V_s placed in a resonant cavity causes the resonant frequency f and quality Q factor to change by a small amount δf . Assuming the shift in frequency is much smaller than the resonant frequency, $\delta f \ll f$, the change in cavity parameters can be expressed as[3, 10, 11, 12]

$$-\frac{\delta \tilde{f}}{f} \simeq \frac{(\tilde{\mu} - 1)\mu_o}{4\langle U \rangle} \int \vec{H} \cdot \vec{H}_o dV_s + \frac{(\tilde{\varepsilon} - 1)\varepsilon_o}{4\langle U \rangle} \int \vec{E} \cdot \vec{E}_o dV_s \quad (1)$$

where the complex frequency shift $\delta \tilde{f} = \delta f - i\Delta f$. $\delta f \equiv f_s - f_c$ and $\Delta f \equiv \Delta f_s - \Delta f_c$ are the changes in the resonant frequency f and the resonance width Δf respectively with (subscript s) and without (subscript c) the sample. The resonance width is related to the cavity Q factor by $\Delta f = f/2Q$. $\langle U \rangle$ is the energy stored in the cavity of the resonant mode. (\vec{H}_o, \vec{E}_o) and (\vec{H}, \vec{E}) are the cavity field configurations before and after the sample perturbation. A time dependence $e^{-i\omega t}$ is assumed. $\tilde{\varepsilon}$ and $\tilde{\mu}$ are the complex permittivity and permeability. We define the magnetic susceptibility as $\tilde{\chi}_M = \tilde{\mu} - 1 = \chi'_M + i\chi''_M$ and the dielectric susceptibility as $\tilde{\chi}_P = \tilde{\varepsilon} - 1 = \chi'_P + i\chi''_P$.

It is convenient to discuss experimental results in terms of an effective dynamic or electromagnetic susceptibility ζ ,

$$\delta \tilde{f} \equiv -g\tilde{\zeta} \equiv -g(\zeta' + i\zeta'') \quad (2)$$

where g is a sample geometrical factor, which is specific to the mode geometry and sample shape. Under appropriate conditions, $\tilde{\zeta}$ can be directly associated with the conventional magnetic $\tilde{\chi}_M$ or dielectric $\tilde{\chi}_P$ susceptibilities, as will be shown below.

To proceed further requires additional assumptions. Various approximations have been made, called the ‘‘Quasistatic’’ (QS), ‘‘Extended Quasistatic’’ (EQS) and Spherical Wave (SW) analysis, depending on the approximation used to obtain the fields (\vec{H}, \vec{E}) . An extensive analysis was carried out by Brodwin and Parsons (BP) [3], which covers essentially all the regimes needed for the experimental measurement discussed here. In the following we use BP and analyze the various regimes.

IV Spherical sample in TE_{011} mode

The TE_{011} configuration is well suited as a probe of the microwave response of materials because of the very high Q ’s achievable in this mode. In the present experiments, the sample is located at the center of the cavity on the axis. In this location we have maximum uniform axial magnetic field \vec{H} and zero electric field \vec{E} . (See Fig.1 for spatial profiles of the \vec{H} and \vec{E} fields). In the following we use the analysis of BP, details of which are given in the appendix.

The geometrical factor g of a spherical sample is given as

$$g = \frac{f}{J_0^2(\beta'_{01}r_o) \left[1 + \left(\frac{\pi}{L\beta'_{01}} \right)^2 \right]} \cdot \frac{V_s}{V_c} \quad (3)$$

where V_c is the volume of the empty cavity. $\beta'_{01}r_o$ is the first root of Bessel function $J'_0(\beta r_o) = 0$. Using the cavity inner radius $r_o = 7/8$ inch, and axial length $L = 1$ inch, we get $g \approx 1.036 \times 10^{15} \cdot V_s$ [$\text{m}^{-3} \cdot \text{sec}^{-1}$], where V_s is the sample volume.

The important parameters that define the analysis are the wave vector inside and outside the sample : $k_o = \omega/c$ and $k = k_o \sqrt{\tilde{\varepsilon} + i\tilde{\sigma}/\omega\varepsilon_o}$. The full-wave analysis yields in principle (see Appendix A), results of the frequency shift due to sample perturbation for a large range of sample sizes and material properties. However in all cases of experimental interest, the sample size is much smaller than the cavity dimensions, so that the condition $k_o a \ll 1$ is rigorously satisfied. For example, if $a = 1\text{mm}$ and the measuring frequency is 10GHz , then $k_o a \simeq 0.2$. In this limit, we obtain

$$\tilde{\zeta}_H = \frac{3}{2} \left(\frac{(2\tilde{\mu} + 1)j_1(ka) - \sin(ka)}{(\tilde{\mu} - 1)j_1(ka) + \sin(ka)} \right) \quad (4)$$

We use the subscript H to denote that the EM susceptibility $\tilde{\zeta}$ is being measured with an applied microwave magnetic field \tilde{H}_ω .

This general form is in principle valid for arbitrary ka which is determined by material properties $\tilde{\mu}$, $\tilde{\varepsilon}$ and $\tilde{\sigma}$. However in this form it is not very useful. It is therefore necessary to consider the different limits of this expression. Below we discuss the various limits and their applicability.

A: Magnetic permeability and susceptibility measurements

More generally the result in this limit can be written as :

$$\tilde{\zeta}_H = 3 \frac{\tilde{\mu} - 1}{\tilde{\mu} + 2} + \frac{9}{10} \left[\frac{\tilde{\mu}^2 - 6\tilde{\mu} + 4}{(\tilde{\mu} + 2)^2} (k_o a)^2 + \frac{\tilde{\mu}}{(\tilde{\mu} + 2)^2} (ka)^2 \right]. \quad (5)$$

Clearly the experiment measures $\tilde{\mu}$ only if the second term is negligible. This may be possible in ferromagnetic samples where $\mu' \gg 1$ provided the spins continue to respond at microwave frequencies. For weakly paramagnetic samples, we have

$$\tilde{\zeta}_H = \tilde{\chi}_M ; \quad (k_o a)^2 \tilde{\chi}_P \ll \tilde{\chi}_M \quad (6)$$

This limit is only achieved provided the sample is highly insulating and the dielectric constant is nearly 1.

A:1 Sensitivity and accuracy of magnetic susceptibility measurements

Having established the relationship between magnetic susceptibility $\tilde{\chi}_M = \chi'_M + i\chi''_M$ and measured electromagnetic susceptibility $\tilde{\zeta}_H$ in Eq. 6, we can estimate the measurement sensitivity of the technique. Clearly the sensitivity is associated with both the size of samples and the cavity resonant frequency f . The bigger the sample size is, the higher the sensitivity is, as seen from Eq.2, 3, 6, provided we still retain the small perturbation limit. Assuming a typical small sample has the dimension of $V_s \sim 1 \times 1 \times 0.5\text{mm}^3$, as in our experiment, we can detect the frequency shift δf and the absorption width Δf as small as 1Hz in a resonant frequency of 10^{10}Hz . This results in a sensitivity limit of $\delta\zeta'_H \sim 10^{-6}$ and hence $\delta\chi'_M \sim 10^{-6}$. For comparison, Table 1 lists the sensitivities of some commonly used techniques for magnetic susceptibility χ measurements[13]. In these measurements, χ generally has the form [13]

$$\chi \approx \frac{M}{V_s H} \quad (7)$$

where M is the magnetic moment in $[A \cdot m^2]$, H is the applied magnetic field in $[A \cdot m^{-1}]$. If the same sample with volume V_s is used for all these measurements, assuming an applied field of $H \simeq 10^5 A/m$ corresponding to typical microwave fields, we can compare their sensitivities, as listed in Table 1. Note that Eq. 6 gives the magnetic volume susceptibility $\tilde{\chi}_M = dM/dH$ in unit of SI or MKS (dimensionless). In CGS, it is usually expressed in $[emu \cdot cm^{-3}]$. To convert from CGS to SI, a conversion multiplying factor of 4π is used.

Method	$M [A \cdot m^2]$	Accuracy in $[m^3/V_s]$	χ value
Superconducting Cavity	—	10^{-16} (in $f \simeq 10GHz$)	relative
dc SQUID	10^{-11}	10^{-16}	absolute
ac - χ	5×10^{-10}	5×10^{-15}	absolute
Vibrating-sample magnetometer	5×10^{-8}	5×10^{-13}	absolute
Alternating-Gradient-Force Magnetometer	10^{-11}	10^{-16}	absolute

Table 1: The comparison of magnetic susceptibility measurements for microwave cavity technique and other techniques.

The table shows that the hot finger cavity perturbation technique undoubtedly has one of the highest measurement sensitivities available. While other methods may require relatively large sample size and large applied field H , these are not required in the microwave measurements. However this high sensitivity is achieved only for relative changes, such as for instance with varying temperature. The precision for absolute measurements is much less due to small uncertainties in sample location.

B: Lossy Dielectric, Permittivity and Surface Impedance Measurements

For even moderate conductivity and dielectric constants, the magnetic contribution is overwhelmed by the dielectric and conductivity contributions. Taking $\tilde{\mu} \sim 1$, in the limit $\tilde{\chi}_M \ll (k_o a)^2 \tilde{\chi}_P$, we have :

$$\tilde{\zeta}_H = -\frac{3}{2} \left(1 - \frac{3}{(ka)^2} + \frac{3 \cot ka}{ka} \right) \quad (8)$$

B.1 Dielectric permittivity and susceptibility measurements

The small ka limit of this results leads directly to a measurement of the dielectric permittivity or susceptibility:

$$\begin{aligned} \tilde{\zeta}_H &\approx \frac{1}{10} (k_o a)^2 (\tilde{\varepsilon} + i\tilde{\sigma}/\omega\varepsilon_o - 1) ; & \tilde{\chi}_M &\ll (k_o a)^2 \tilde{\chi}_P, \quad ka \ll 1 \\ &\approx \frac{1}{10} (k_o a)^2 \tilde{\chi}_P ; & \tilde{\sigma} = 0, \tilde{\chi}_M &\ll (k_o a)^2 \tilde{\chi}_P, \quad ka \ll 1 \end{aligned} \quad (9)$$

A surprising conclusion is that *one can measure the dielectric properties even though the sample is placed in a pure microwave magnetic field*. We emphasize that this conclusion has nothing to do with the spatial variation of the E -field near the cavity axis. It simply arises from the wave equation and *holds, within geometric factors, even in a homogenous magnetic field and with zero electric field*, such as can be achieved in a split ring resonator [6].

This method of measuring $\tilde{\varepsilon}$ has one important advantage over E -field cavity perturbation measurements. The measured quantity is directly proportional to $\tilde{\varepsilon} - 1$ and holds even when $\tilde{\varepsilon} \gg 1$ so long as $(k_o a)^2 (\tilde{\varepsilon} - 1) < 1$, while in the E -field method the measured frequency shifts are proportional to $(\tilde{\varepsilon} - 1)/(\tilde{\varepsilon} + 2)$, due to so-called depolarization effects (see Appendix B), and can obscure the direct interpretation of the results.

For general $\tilde{\varepsilon}$ Eq.8 can be inverted to obtain $\tilde{\varepsilon}$ from the measured $\tilde{\zeta}_H$. Examples of such inversions are presented later.

Note that the dielectric permittivity measured is that appropriate to the plane perpendicular to the direction of the magnetic field \vec{H}_ω . This is the direction of the displacement currents, and also the induced conduction currents. If the response in the plane is anisotropic then the measured $\tilde{\epsilon}$ will be an appropriate mixture of the responses in the different axes in the perpendicular plane. This must be viewed as a drawback compared to the E-field method, where in principle the response along each axis can be measured using a needle shaped specimen.

B:.2 Surface Impedance measurements (skin depth or eddy current limit)

The other useful limit is for a highly conducting material, where $ka = (1+i)a/\delta = (1+i)a\sqrt{\mu_o\omega\sigma}$. The skin depth $\delta = 1/\sqrt{\mu_o\sigma\omega} \ll a$, hence

$$\tilde{\zeta}_H - \zeta'_{H\infty} = \frac{3}{\mu_o\omega a}(X_s + iR_s) ; \quad \text{when } \tilde{\chi}_M \sim 0, a \gg \delta, ka \gg 1 \quad (10)$$

It is useful to reference the data to the complete diamagnetic result $\zeta'_{H\infty} = -1.5$ for a sphere. Thus in this limit the data are a direct measure of the surface impedance

$$\tilde{Z}_s = R_s - iX_s = \sqrt{\frac{-i\omega\mu_o}{\tilde{\sigma}}} \quad (11)$$

The normalization factor $3/(\mu_o\omega a)$ is specific to the spherical sample and TE_{011} mode geometries. Note that in this limit the measured data are $\propto 1/\sqrt{\sigma}$.

It is worth noting that this result (Eq.11) is also valid for complex conductivity $\tilde{\sigma} = \sigma_1 + i\sigma_2$ such as for a superconductor. The above treatment assumes that displacement current effects are negligible. If they are also present and can be represented in terms of a dielectric constant $\tilde{\epsilon}$, then we can also write

$$\tilde{Z}_s = R_s - iX_s = \sqrt{\frac{-i\omega\mu_o}{\tilde{\sigma} - i\omega\tilde{\epsilon}}} \quad (12)$$

B:.3 Conductivity (Eddy Current) Peaks and Dielectric Loss Peaks

As noted above, the measured changes in the cavity resonance parameters expressed here in terms of the electromagnetic susceptibility $\tilde{\zeta}_H$ change from a $\propto \sigma$ dependence for small σ to a $\propto 1/\sqrt{\sigma}$ dependence for large σ . Thus as σ is varied this results in a peak in the absorption or in ζ''_H , accompanied by a change of state of ζ'_H from 0 to $\zeta'_{H\infty} = -1.5$, as shown in Fig.2. This conductivity or eddy current peak is similar to the depolarization peak observed in E -field measurements. Of course the location of the conductivity peak is determined by both the conductivity and the sample dimensions.

In certain materials, particularly the oxides, there are dielectric loss peaks intrinsic to the material, arising from a dielectric constant $\tilde{\epsilon} = \epsilon' + i\epsilon'' = \epsilon(0)/(1+i\omega\tau)$. Usually τ is a strong function of temperature T , and hence when T is varied, a peak in $\epsilon''(T)$ occurs at a peak temperature T_p where $\omega\tau(T_p) = 1$. Since $\tau(T)$ increases with decreasing T , this peak shifts to lower peak temperatures T_p when the measurement frequency is decreased. Since $\tilde{\zeta}_H$ is proportional to $\tilde{\epsilon}$ in the appropriate limit, a peak will be observed in ζ''_H also as T is varied.

In such materials $\sigma(T)$ is also a strong function of T and typically is semiconducting : $\sigma(T) = \sigma_o \exp(-T_{s0}/T)$. Under such conditions, the experimental data will display two peaks, one a dielectric loss peak and the other a conductivity peak, as T is varied. When the measuring frequency ω is reduced, the dielectric loss peak will move to lower T while the conductivity peak will move to higher T , i.e. the peaks move apart on the T axis with decreasing ω . A specific example of a dielectric loss peak in the spin ladder material $Sr_{14}Cu_{24}O_{41}$ is discussed later.

B:.4 Dimensional Resonances

A remarkable prediction of Eq.8 is the occurrence of dimensional resonances when the dielectric constant varies strongly. This is shown in Fig.3 (a) and (b). The resonances occur whenever

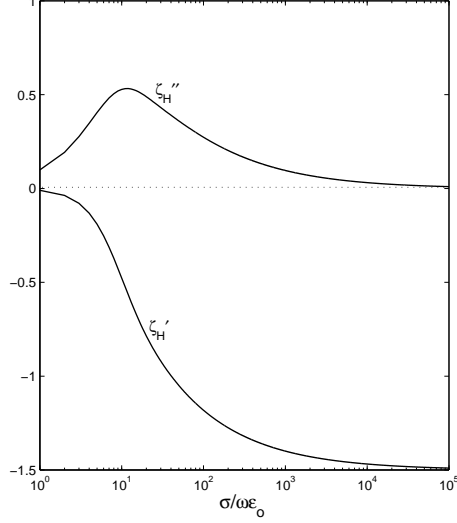


Figure 2: ζ_H' and ζ_H'' vs. $\sigma/i\omega\epsilon_0$ showing the conductivity peak as σ is varied.

$ka = (n + 1/2)\pi$ and are quite sharp. They correspond to situations where the electromagnetic field essentially resonates inside the sample, just like a dielectric resonator. We have observed such resonances in $SrTiO_3$, which can be viewed as a quantum paraelectric with transition temperature at $T = 0$, and in which material ϵ' increases rapidly with decreasing T to values approaching several thousands. Results are discussed later.

V Experimental Procedures

In the experiment, we first carry out a background run to measure the resonance frequency $f_c(T)$ and the width $\Delta f_c(T)$ of the empty cavity as a function of T . Then the sample is inserted in and corresponding parameters $f_s(T)$ and $\Delta f_s(T)$ are measured. $\tilde{\zeta}_H = \zeta_H'(T) + i\zeta_H''(T)$ is obtained using

$$\begin{aligned}\zeta_H'(T) &= -\frac{1}{g}(f_s(T) - f_c(T)) \\ \zeta_H''(T) &= \frac{1}{g}(\Delta f_s(T) - \Delta f_c(T)).\end{aligned}\tag{13}$$

g is given by Eq. 3. In practice, while relative changes $\delta f_s(T) = f_s(T) - f_s(T_{ref})$ or $\delta f_c(T) = f_c(T) - f_c(T_{ref})$ referred to a reference temperature T_{ref} can be measured with extremely high precision, there can be larger errors in the absolute value of $f_s(T) - f_c(T)$. For this reason we represent the data as

$$\zeta_H'(T) = -\frac{1}{g}[(\delta f_s(T) - \delta f_c(T)) + \delta f(T_{ref})]\tag{14}$$

In many cases, the background correction $\delta f_c(T)$ can be negligible. It is convenient to present the data as $\delta\zeta_H'(T) = \zeta_H'(T) - \zeta_H'(T_{ref})$ instead of $\zeta_H'(T)$. To get the absolute value of ζ_H' , calibration can be made by putting the sample into the cavity to measure f_s and then immediately taking the sample out to measure f_c at a fixed temperature, and thus obtain $\delta f(T_{ref})$. For many samples, (e.g. see $Sr_{14}Cu_{24}O_{41}$ later), $\zeta_H'(T_{ref}) \ll \zeta_H'(T)$ particularly at high T , so that in these cases, $\delta\zeta_H' \approx \zeta_H'$.

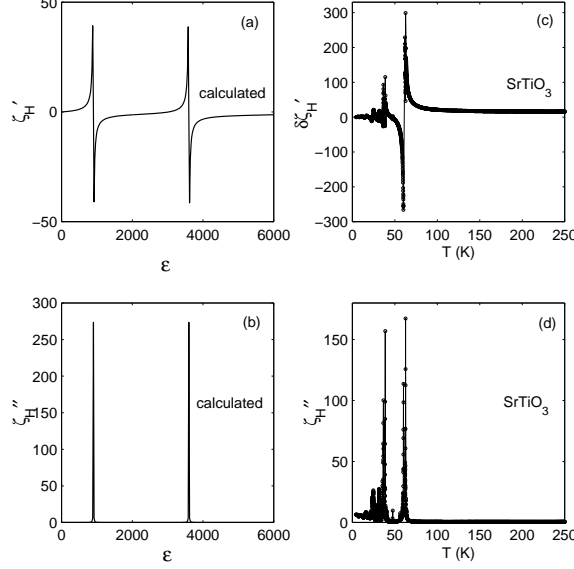


Figure 3: (a) ζ'_H and (b) ζ''_H vs. ε calculated using Eq. 8. The plots show the dimensional resonances which occur when $ka = (n + 1/2)\pi$. Experimental data of (c) $\delta\zeta'_H$ and (d) ζ''_H vs. T for $SrTiO_3$. The dimensional resonances, similar to (a) and (b), are clearly visible. In this material the dielectric constant ε' increases with decreasing T .

A: Inversion of experimental $\tilde{\zeta}$ or \tilde{Z}_s data to obtain $\tilde{\varepsilon}$ and $\tilde{\sigma}$

The next key step is to obtain the fundamental material property, the sample dielectric function $\tilde{\varepsilon}$ or conductivity $\tilde{\sigma}$, from the experimental data represented either as $\tilde{\zeta}$ or the surface impedance \tilde{Z}_s . Two approaches are possible here :

1. A direct inversion of Eq.8 for $\tilde{\zeta}(T)$ data or Eq.11 for $\tilde{Z}_s(T)$ data to extract $\tilde{\sigma}(T) - i\omega\tilde{\varepsilon}(T)$,
2. Modelling of $\tilde{\sigma}(T) - i\omega\tilde{\varepsilon}(T)$ to quantitatively match the $\tilde{\zeta}(T)$ data using Eq.8 or $\tilde{Z}_s(T)$ data using Eq.11.

We discuss both these procedures below.

A:.1 Inversion of equations

We have successfully solved Eq.8 to obtain $\tilde{z} = ka = k_o a \sqrt{\tilde{\varepsilon} + i\tilde{\sigma}/\omega\varepsilon_o}$ using the subroutine *FSOLVE* in MATLAB. The success of the solution depends crucially on the values of $\tilde{\zeta}$ or equivalently \tilde{z} . For values of $\zeta', \zeta'' \sim 1$, which is well in the QS or EQS limits, the solution is very accurate and yields the sample $\tilde{\sigma} - i\omega\tilde{\varepsilon}$ with ease. In this limit $\tilde{z} \lesssim 1$, corresponding to typical dielectric constants $\varepsilon' \leq 1000$ (for the sample and cavity sizes discussed in this paper) and not too small ε'' . Thus for lossy dielectrics, the results for $\tilde{\varepsilon}$ can be easily obtained. The results of such a solution for the material $Sr_{14}Cu_{24}O_{41}$ are discussed later in this paper. Results on several other materials which have similar properties, such as $La_{5/3}Sr_{1/3}NiO_4$, $YBa_2Cu_3O_{6.0}$ and $PrBa_2Cu_3O_{7.0}$, are described in previous and forthcoming papers [14, 15].

Great care must be exercised in two regimes of parameter values :

1. when $\zeta' \gg 1$, and $\zeta'' \leq 1$, which corresponds to $ka \gg 1$ ($\varepsilon' > 1000$ for the conditions of the experiments in this paper). Here the resonances of $\cot(z)$ enter when $ka = (n + 1)\pi/2$, leading to dimensional resonances discussed in other sections.

2. the metallic limit, when $\zeta' \rightarrow -1.5$, and $\zeta'' \ll 1$. In this limit it is more appropriate to use the surface impedance limit Eq.11 rather than Eq.8.

The principal difficulty in the above two limits is that there are many nearby minima of the underlying function, and the program quickly converges to spurious solutions. Future work will focus on this important problem.

A.2 Modelling the conductivity and dielectric constant to match the data

Even if the solution procedure is successful and the material $\tilde{\sigma} - i\omega\tilde{\epsilon}$ is successfully extracted, a quantitative understanding of the experimental results for $\tilde{\sigma} - i\omega\tilde{\epsilon}$ requires a model. Where the solution is not easily attained due to the difficulties mentioned above, we have found it necessary to bypass the solution procedure and instead use model calculations of $\tilde{\sigma} - i\omega\tilde{\epsilon}$ to describe the $\tilde{\zeta}$ data using Eq.8 and Eq.11.

VI Experimental Results

We describe below measurements on three different materials all in single crystal form. These crystals have typical dimensions of $1 \times 1 \times 0.5 \text{ mm}^3$ and have been extensively characterized by a vast array of measurements: dc resistivity, dc SQUID susceptibility, XRD, neutron scattering and high pressure studies. Structural studies of the single crystals show that of all of these measurements indicate single phase, high quality crystals.

A: Magnetodynamics in the spin chain material Sr_2CuO_3

Sr_2CuO_3 single crystals were prepared by the floating zone technique[16]. It is an insulator in a large range of temperature and there is only possesses linear $\text{Cu} - \text{O}$ chains and is regard as an ideal one-dimensional spin 1/2 chain. In the measurement, the sample is mounted in such way that the microwave field $H_\omega // \hat{c}$ -axis. Fig.4 (a) shows the plot of $\delta\zeta'_H(T) \equiv \zeta'_H(T) - \zeta'_H(2K)$ vs. T and $\zeta''_H(T)$ vs. T for Sr_2CuO_3 . $\delta\zeta'_H$ shows a monotonic increase with temperature T , and ζ''_H has insignificant changes from 6K to 260K. These results are consistent with the DC magnetic susceptibility measurements [17], as shown in dashed line of Fig.4 (a), and indicate that the sample perturbation effect is in the magnetic susceptibility limit $(k_o a)^2 \tilde{\chi}_P \ll \tilde{\chi}_M$, so that $\tilde{\zeta}_H \simeq \tilde{\chi}_M$. Thus in this material we are essentially measuring the magnetic susceptibility.

At low temperatures, additional features are observed in both $\delta\zeta'_H$ and ζ''_H , as shown in Fig.4 (b) and (c). These peaks are microwave signatures of the 3D Heisenberg AFM transition at $T_N \approx 5K$ [17]. The very high sensitivity of the technique utilizing a superconducting cavity is evident from the data in Fig.4.

B: Dielectric Loss Peaks in the spin ladder material $\text{Sr}_{14}\text{Cu}_{24}\text{O}_{41}$

There is increasing interest for studying spin/ladder compounds because superconductivity can be obtained in Ca doped $\text{Sr}_{14}\text{Cu}_{24}\text{O}_{41}$ under high pressures[18]. In Fig. 5, we show the results of $\tilde{\zeta}(T)$ in the case of $H_\omega // \hat{c}$ -axis for $\text{Sr}_{14}\text{Cu}_{24}\text{O}_{41}$. The striking feature of the data is the rapid drop with decreasing T in $\delta\zeta''_H(T)$ below approximately 200K, accompanied by a relatively sharp peak in $\zeta''_H(T)$ at $T \sim 170K$, which is not seen in the DC magnetic susceptibility measurement (Fig.5 (b)).

The extraordinary dynamic range (over 4 orders of magnitude in $\tilde{\zeta}_H$) of the superconducting cavity enables us to see an additional peak at low T in Fig.5 (b) (the semilog plot of (a) data). Although a similar peak is also observed in $\chi_{dc}(T)$, the magnitude is about 10 times smaller than $\zeta''_H(T)$. At high temperatures, the measured $\zeta'_H/\chi_{dc} \sim 10^3$. Thus in this material the dielectric contributions dominate, i.e. $(k_o a)^2 \tilde{\chi}_P \gg \tilde{\chi}_M$, and we are thus measuring the dielectric constant.

Fig.5 (c) shows the dielectric constant ϵ' and ϵ'' obtained from the measured $\tilde{\zeta}$ data and inverting Eq.8. The loss peak in ϵ'' is clearly evident, and is accompanied by a change of state of ϵ' . These data indicate an essentially pure dielectric relaxation process in this spin ladder material, arising from the presence of charges due to doping.

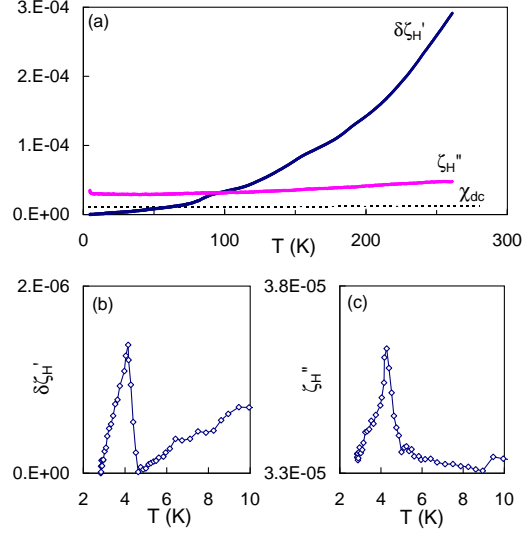


Figure 4: (a) Measured microwave magnetic susceptibility $\tilde{\zeta}_H$ vs. T for Sr_2CuO_3 . For this sample the limit $\tilde{\zeta}_H \approx \tilde{\chi}_M$ applies. Also shown is the dc susceptibility (dashed line) from [17]. (b) and (c) are low T data of $\delta\zeta_H'$ and ζ_H'' , showing signatures of the 3-D AFM transition at $T \sim 5K$.

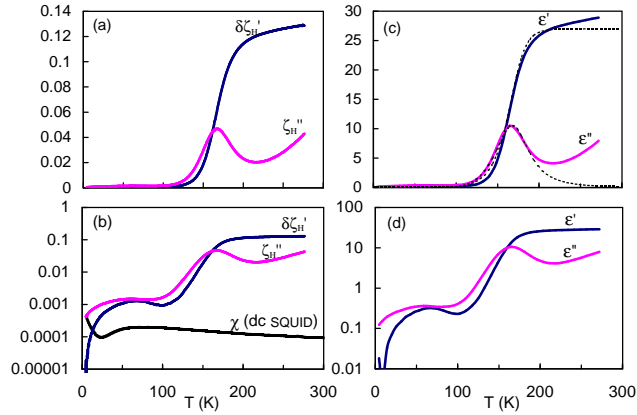


Figure 5: Experimental data of $\delta\zeta_H'$ ($\approx \zeta_H'$) and ζ_H'' for $Sr_{14}Cu_{24}O_{41}$ in (a) linear and (b) semilog plots. (c) ϵ' and ϵ'' obtained from the $\tilde{\zeta}_H$ data of (a) by solving Eq. 8. The dielectric loss peak is clearly evident. Also shown in (c) (dashed line) is the fit of the dielectric response to a Cole-Davidson form. (d) Data of (c) in a semilog plot, showing an additional feature at 110K coincident with the opening of the magnetic gap reported in this system.

The dielectric mode is well described by a Cole-Davidson form $\tilde{\varepsilon}(\omega, T) = \varepsilon(0)/[1 + i\omega\tau(T)]^\beta$, with $\varepsilon(0) = 27$, $\beta = 0.6$ and an activated relaxation time $\tau(T) = 1.6 \times 10^{-16} \cdot \exp(T_{\tau 0}/T)$ [sec.], with an activation energy $T_{\tau 0} = 2000K$. When the relaxation rate $\tau^{-1}(T)$ varies rapidly with T and crosses the measurement frequency ω , a peak occurs at T_p , where $\omega\tau(T_p) = 1$, as shown in Fig.5. In this material the relaxation time $\tau(T)$ appears to follow the conductivity $\sigma(T)$, indicating that the free carriers determine the polarization relaxation. Extensive details of the polarization dynamics in this material and in the related $Sr_{14-x}Ca_xCu_{24}O_{41}$ family are discussed in a forthcoming publication [9].

C: Dimensional resonances in $SrTiO_3$

One of the striking predictions of the above analysis is the occurrence of dimensional resonances discussed in an earlier section. These resonances occur when the dielectric constant is so large that the condition $ka = (n + 1/2)\pi$ is satisfied. We have experimentally observed such resonances in single crystal samples of $SrTiO_3$ measured in a TE_{011} cavity. The single crystal samples were purchased from Aesar Mfg. Co.. The experimental data are shown in Fig.3 (c) and (d), where $\delta\zeta'_H(T)$ and $\zeta''_H(T)$ are shown as a function of T for a sample with dimensions $0.5 \times 0.5 \times 0.5mm^3$. The data clearly show resonances as a function of T . In this material ε' increases strongly with decreasing T approaching values of nearly 1000. The experimental data shown in Fig.3 (c) and (d) are quantitatively consistent with the behavior in (a) and (b).

Inversion of Eq.8 shows a weakly T -dependent $\varepsilon' \sim 850$ between $250K$ and about $75K$. This value is entirely consistent with other measurements [19]. However at lower temperatures the inversion of the ζ_H data to obtain $\tilde{\varepsilon}$ is problematical because of the dimensional resonances. Here as noted before the solutions do not appear to be unique and spurious solutions are found.

An important parameter for microwave applications is the microwave loss in $SrTiO_3$. We find that $\varepsilon''(T)$ varies between $0.1 - 0.25$ in the temperature region between $250K$ and about $75K$ where smooth solutions of $\varepsilon' \sim 850$ are obtained. We also note that the raw experimental data for $\tilde{\zeta}$ indicate that the biggest resonances occur at $62K$ and $37K$ which is exactly where dielectric anomalies have been reported in lower temperature measurements [19].

D: Conclusion

We have shown that a careful analysis of cavity perturbation methods, combined with the use of superconducting cavities, leads to a powerful method of measuring transport properties at microwave frequencies. The method can lead to exceptionally high sensitivities for the material properties.

A surprising result is that dielectric constants can be measured even though the sample is placed in a microwave magnetic field. One consequence of this conclusion is that many such experiments which use samples in microwave magnetic fields, such as non-resonant microwave absorption measurements [20], should be carefully analyzed for the influence of dielectric properties, and not just the magnetic properties.

The resulting microwave measurements show new dynamic phenomena with time scales corresponding to the GHz frequency ranges which is not seen in static dc SQUID susceptibility measurements. The microwave measurements yield information on dynamics at time scales $\sim 10^{-11}$ sec., comparable to NS, but shorter than NMR and NQR (10^{-7} sec.) and μSR (10^{-8} sec.), and are a sensitive probe of charge dynamics novel electronic materials. These results will lead us to a new perspective of how to understand other cuprates. In future publications, we will discuss the results of measurements on low dimensional spin systems and high temperature superconductors.

We thank A. Revcolevschi for providing samples of Sr_2CuO_3 and $Sr_{14}Cu_{24}O_{41}$, and R. S. Markiewicz for useful discussions. This research was supported by NSF-9711910, AFOSR-F30602-95-2-0011 and ONR-N00014-00-1-0002.

References

- [1] S. Sridhar and W. Kennedy, Rev. Sci. Instr. **59**, 531 (1988).

- [2] G. Grüner, ed. “*Millimeter and Submillimeter Wave Spectroscopy of Solids*”, Springer (1998).
- [3] M. E. Brodwin and M. K. Parsons, J. App. Phys. **36**, 494 (1965).
- [4] S. K. Khanna, E. Ehrenfreund, A. E. Garito and A. J. Heeger, Phys. Rev. B **10**, 2205 (1974).
- [5] N. P. Ong, J. App. Phys. **48**, 2935 (1977).
- [6] D. A. Bonn, D. C. Morgan, and W. N. Hardy, Rev. Sci. Instr. **62**, 1819 (1991)
- [7] J. C. Booth, D. H. Wu, and S. M. Anlage, Rev. Sci. Instr. **65**, 2082 (1994).
- [8] T. Jacobs, et al., Rev. Sci. Instr. **67**, 3757 (1996).
- [9] Z. Zhai, et. al., Physica C, **282-287**, 1601 (1997).
- [10] J. Muller, Z. Hochfr. Techn. Elektr. **54**, 157 (1939).
- [11] J. C. Slater, Rev. Mod. Phys. **18**, 441 (1946).
- [12] D.-N. Peligrad, B. Nebendahl, C. Kessler and M. Mehring, Phys. Rev. B **58**, 11652 (1998).
- [13] R. B. Goldfarb, M. Lelental and C. A. Thompson in *Magnetic Susceptibility of Superconductors and Other Systems*, edit by R. A. Hein, T. L. Francavilla, and D. H. Liebenberg, Plenum Press, New York (1991).
- [14] Hakim et al, 1999 Fall MRS proc. (submitted).
- [15] Z. Zhai, S. Sridhar, et. al, (to be published).
- [16] A. Revcolevschi, et. al., Physica **C 282-287**, 493 (1997).
- [17] N. Motoyama, H. Eisaki, S. Uchida, Phys. Rev. Lett. **76**, 3212 (1996).
- [18] M. Uehara, et. al., J. Phys. Soc. Japan, **65**, 2764 (1996).
- [19] Chen Ang, J. F. Scott, Zhi Yu, H. Ledbetter and J. L. Baptista, Phys. Rev. **B 59**, 6661 (1999).
- [20] A. Narlikar, ed. “*Microwave Studies of High Temperature Superconductors*”, Vol 18, Nova Science Publishers (1996).
- [21] J. A. Stratton, *Electromagnetic Theory*, McGraw-Hill Book Company, New York (1941).

A Spherical sample in magnetic field maximum of TE_{011} mode

Brodwin and Parsons treated a spherical homogeneous sample with radius a in a resonant cavity when the restrictions $ka \ll 1$ and $k_o a \ll 1$ are removed. They use a method developed by Stratton[21] in which the electric and magnetic fields inside and outside the perturbing sample are expressed as expansions of spherical vector potential functions.

The field configurations of the TE_{011} mode in cylindrical coordinate $(\hat{r}, \hat{\phi}, \hat{z})$ are expressed as

$$\begin{aligned}\vec{H}(r, \varphi, z) &= -H_o \frac{\pi}{\beta'_{01} L} J_1(\beta'_{01} r) \cos\left(\frac{\pi z}{L}\right) \hat{r} + H_o J_0(\beta'_{01} r) \sin\left(\frac{\pi z}{L}\right) \hat{z} \\ \vec{E}(r, \varphi, z) &= H_o \frac{i\omega\mu_o}{\beta'_{01}} J_1(\beta'_{01} r) \sin\left(\frac{\pi z}{L}\right) \hat{\phi}\end{aligned}\quad (15)$$

where H_o is the maximum magnetic field in the center of the cavity, r_o is the radius of the cavity, L is the cavity axial length, and $\beta'_{01} r_o$ is the first root of the Bessel function $J'_0(\beta r_o) = 0$. A time dependence $e^{-i\omega t}$ is assumed in \vec{H} and \vec{E} . When a small sample with radius a is put inside the cavity, the complex frequency shift $\delta\tilde{\omega}$ for TE_{011} mode is given by the following expression[3]

$$\frac{\delta\tilde{\omega}}{\omega} = \frac{i9\eta \sin^2 \alpha}{2J_0^2(\beta'_{01} r_o)} \sum_{n=1}^{\infty} \frac{2(2n+1)}{3n(n+1)} \left[\frac{P'_n(\cos \alpha)}{\sin \alpha} \right]^2 \delta_{0n} \left(\frac{a_n^r}{\rho^3} \right) \quad (16)$$

where $\beta = \sqrt{k_o^2 - h^2} = \kappa_o \sin \alpha$, $h = \pi/L$, and $\eta = V_s/V_c$ is the filling factor. a_n^r is the coefficient corresponding to the reflected (scattered) field and is given by the following expression with $\rho = k_o a$ and $N\rho = ka$ [3].

$$a_n^r = \frac{-\tilde{\mu} j_n(N\rho) [\rho j_n(\rho)]' + j_n(\rho) [N\rho j_n(N\rho)]'}{\tilde{\mu} j_n(N\rho) [\rho h_n^1(\rho)]' - h_n^1(\rho) [N\rho j_n(N\rho)]'} \quad (17)$$

In the following we define the sample geometrical factor γ as

$$\gamma = \frac{\eta \sin^2 \alpha}{J_0^2(\beta'_{01} r_o)} \quad (18)$$

Considering the cavity resonant frequency $\omega_{mnp} = c\sqrt{\beta'^2_{mn} + p^2\pi^2/L^2}$, γ for the TE_{011} mode can be rewritten as

$$\gamma = \frac{\eta}{J_0^2(\beta'_{01} r_o) \left[1 + \left(\frac{\pi}{\beta'_{01} L} \right)^2 \right]} \quad (19)$$

This series in Eq.16 is rapidly convergent for samples with diameters less than $\lambda/2\pi$, therefore the leading term give a good approximation for the frequency shift.

$$\frac{\delta\tilde{\omega}}{\omega} = \frac{i9\gamma a_1^r}{2\rho^3} \quad (20)$$

Using the spherical Bessel functions: $j_1(\rho) = [\sin(\rho) - \rho \cos(\rho)]/\rho^2$, $h_1^{(1)}(\rho) = -e^{i\rho}(\rho + i)/\rho^2$, and $[\rho j_1(\rho)]' = -[\sin(\rho) - \rho \cos(\rho)]/\rho^2 + \sin(\rho)$, we can examine the results of $\delta\tilde{\omega}$ in various limits.

A: Extended Quasistatic Limit $k_o a \ll 1$

In this approximation, $j_1(\rho) = \rho/3 - \rho^3/30$, $h_1^{(1)}(\rho) = -i/\rho^2 - i/2 + \rho/3 + O(3)$, and $[\rho j_1(\rho)]' = 2\rho/3 - 2\rho^3/15$, $[\rho h_1^{(1)}(\rho)]' = i/\rho^2 - i/2 + 2\rho/3 + O(3)$, Eq.16 can be written as

$$\frac{\delta\tilde{\omega}}{\omega} = -\frac{3\gamma}{2} \left[\frac{2\tilde{\mu} j_1(N\rho) - [N\rho j_1(N\rho)]'}{\tilde{\mu} j_1(N\rho) + [N\rho j_1(N\rho)]'} \right] + A_1 \cdot (k_o a)^2 \quad (21)$$

where A_1 is coefficient of the second order term of $k_o a$ and given by:

$$A_1 = \frac{3\gamma}{20} \left[\frac{4\tilde{\mu}j_1(N\rho) - [N\rho j_1(N\rho)]'}{\tilde{\mu}j_1(N\rho) + [N\rho j_1(N\rho)]'} \right] - \frac{3\gamma}{4} \left[\frac{\left(2\tilde{\mu}j_1(N\rho) - [N\rho j_1(N\rho)]' \right) \left(\tilde{\mu}j_1(N\rho) - [N\rho j_1(N\rho)]' \right)}{\left(\tilde{\mu}j_1(N\rho) + [N\rho j_1(N\rho)]' \right)^2} \right] \quad (22)$$

A.:1 Quasistatic Limit $k_o a \ll 1$

Considering $N\rho = ka \ll 1$ the frequency shift $\delta\tilde{\omega}$ can be reduced to:

$$\frac{\delta\tilde{\omega}}{\omega} = -3\gamma \frac{\tilde{\mu} - 1}{\tilde{\mu} + 2} - \frac{9\gamma}{10} \left[\frac{\tilde{\mu}^2 - 6\tilde{\mu} + 4}{(\tilde{\mu} + 2)^2} (k_o a)^2 + \frac{\tilde{\mu}}{(\tilde{\mu} + 2)^2} (ka)^2 \right] \quad (23)$$

If $\tilde{\mu} = 1 + \tilde{\chi}_m \approx 1$, in addition to $k_o a, ka \ll 1$, then the above equation reduces to

$$\begin{aligned} \frac{\delta\tilde{\omega}}{\omega} &\approx -\gamma(\tilde{\mu} - 1) \\ &= -\gamma\tilde{\chi}_M = -\gamma(\chi_M' + i\chi_M'') \end{aligned} \quad (24)$$

Here the frequency shift $\delta\tilde{\omega}$ is a measurement of the complex magnetic susceptibility $\tilde{\chi}_M$.

A.:2 Pure conductor: Eddy current or skin depth limit: $\tilde{\mu} = 1, \tilde{\varepsilon} = 1, \tilde{\sigma} = \sigma$

In this limit $ka = (1 + i)a/\delta$, where $\delta = 1/\sqrt{\mu_o \tilde{\sigma} \omega}$ is the skin depth. Retaining the first order in the series of Eq.21, we obtain the complex frequency shift $\delta\tilde{\omega}$:

$$\begin{aligned} \frac{\delta\tilde{\omega}}{\omega} &= -\frac{3\gamma}{2} \left[\frac{2j_1(N\rho) - [N\rho j_1(N\rho)]'}{j_1(N\rho) + [N\rho j_1(N\rho)]'} \right] \\ &\approx \frac{3\gamma}{2} \left[1 - \frac{3}{(ka)^2} + \frac{3 \cot ka}{ka} \right] \end{aligned} \quad (25)$$

By using $\cot(x + iy) = \sin 2x/(\cosh 2y - \cos 2x) - i \sinh 2y/(\cosh 2y - \cos 2x)$, we obtain the following expressions:

$$\begin{aligned} \text{Re} \left(\frac{\delta\tilde{\omega}}{\omega} \right) &= \frac{3\gamma}{2} \left[1 - \frac{3}{2} \left(\frac{\delta}{a} \right) \left(\frac{\sinh \frac{2\delta}{a} - \sin \frac{2\delta}{a}}{\cosh \frac{2\delta}{a} - \cos \frac{2\delta}{a}} \right) \right] \\ \text{Im} \left(\frac{\delta\tilde{\omega}}{\omega} \right) &= \frac{9\gamma}{4} \left(\frac{\delta}{a} \right)^2 \left[1 - \left(\frac{a}{\delta} \right) \left(\frac{\sinh \frac{2\delta}{a} + \sin \frac{2\delta}{a}}{\cosh \frac{2\delta}{a} - \cos \frac{2\delta}{a}} \right) \right] \end{aligned} \quad (26)$$

In the low frequency limit where $\delta \gg a$ the above formulas become:

$$\begin{aligned} \text{Re} \left(\frac{\delta\tilde{\omega}}{\omega} \right) &= \frac{4\gamma}{105} \left(\frac{\delta}{a} \right)^4 \\ \text{Im} \left(\frac{\delta\tilde{\omega}}{\omega} \right) &= \frac{\gamma}{5} \left(\frac{\delta}{a} \right)^2 \end{aligned} \quad (27)$$

In the high frequency limit where $\delta \ll a$ we obtain the expressions:

$$\begin{aligned} \text{Re} \left(\frac{\delta\tilde{\omega}}{\omega} \right) &= \frac{3\gamma}{2} - \frac{9\gamma}{4} \left(\frac{\delta}{a} \right) \\ \text{Im} \left(\frac{\delta\tilde{\omega}}{\omega} \right) &= \frac{9\gamma}{4} \left(\frac{\delta}{a} \right) \end{aligned} \quad (28)$$

Therefore the complex frequency shift $\delta\tilde{\omega}$ could be written in terms of surface impedance $Z_s = R_s - iX_s$:

$$\frac{\delta\tilde{\omega}}{\omega} = \frac{3\gamma}{2} \left[1 - \frac{3}{\omega\mu_o a} (X_s + iR_s) \right] \quad (29)$$

with $R_s = X_s = \sqrt{\omega\mu_o/2\sigma}$.

A.3 Lossy Dielectric : $\tilde{\mu} = 1$, $\tilde{\varepsilon} = \varepsilon' + i\varepsilon''$, $\tilde{\sigma} = \sigma$.

In this case, $k^2 = (\omega/c)^2(\tilde{\varepsilon} + i\tilde{\sigma}/\omega\varepsilon_o)$, the frequency shift has a similar expression with the one derived for a perfect conductor but in this case the real and the imaginary part of the wave vector are not equal.

$$\frac{\delta\tilde{\omega}}{\omega} = \frac{3\gamma}{2} \left[1 - \frac{3}{(ka)^2} + \frac{3 \cot ka}{ka} \right] \quad (30)$$

In the limit where $ka \ll 1$, the above equation can be written as

$$\begin{aligned} \frac{\delta\tilde{\omega}}{\omega} &\approx -\frac{\gamma}{10} (k_o a)^2 (\tilde{\varepsilon} + i\frac{\tilde{\sigma}}{\omega\varepsilon_o} - 1) \\ &\approx -\frac{\gamma}{10} (k_o a)^2 \tilde{\chi}_P ; \quad (\text{when } \tilde{\sigma} = 0) \end{aligned} \quad (31)$$

where $\tilde{\chi}_P \equiv \tilde{\varepsilon} - 1 = \varepsilon' - 1 + i\varepsilon'' = \chi'_P + i\chi''_P$. Here the frequency shift $\delta\tilde{\omega}$ is a measurement of the complex dielectric susceptibility $\tilde{\chi}_P$ when $\tilde{\sigma} = 0$.

B Sample in TM_{110} Electric Field Maximum

Although we have focussed on the TE_{011} mode, it is also possible to carry out measurements using the TM_{110} mode. For a sample placed in the cavity center at the microwave electric field maximum, the frequency shift is [3]:

$$\frac{\delta\tilde{\omega}}{\omega} = \frac{i9\eta}{4J_1^2(\beta'_{01}r_o)} \sum_{n=1}^{\infty} \frac{2(2n+1)}{3n(n+1)} [P'_n(0)]^2 \delta_{0n} \left(\frac{b_n^r}{\rho^3} \right) \quad (32)$$

with the reflection coefficient [3]:

$$b_n^r = \frac{-\tilde{\varepsilon} j_n(N\rho) [\rho j_n(\rho)]' + j_n(\rho) [N\rho j_n(N\rho)]'}{\tilde{\varepsilon} j_n(N\rho) [\rho h_n^1(\rho)]' - h_n^1(\rho) [N\rho j_n(N\rho)]'} \quad (33)$$

In the first order the Eq.32 becomes:

$$\frac{\delta\tilde{\omega}}{\omega} = -\frac{3\gamma'}{2} \left(\frac{2\tilde{\varepsilon} j_1(N\rho) - [N\rho j_1(N\rho)]'}{\tilde{\varepsilon} j_1(N\rho) + [N\rho j_1(N\rho)]'} \right) \quad (34)$$

with a new geometrical factor γ' given by:

$$\gamma' = \frac{\eta}{2J_1^2(\kappa_{01}r_o)} \quad (35)$$

where $\kappa_{01}r_o$ is the first root of the Bessel function $J_0(\kappa r_o) = 0$

In the limit where $ka \ll 1$ the frequency shift is:

$$\frac{\delta\tilde{\omega}}{\omega} = -3\gamma' \frac{\tilde{\varepsilon} - 1}{\tilde{\varepsilon} + 2} + O(2) \quad (36)$$